Journal of Materials Chemistry A

Accepted Manuscript

ROYAL SOCIETY OF CHEMISTRY

www.rsc.org/materialsA

Journal Name

Dynamic Article Links ►

Cite this: DOI: 10.1039/c0xx00000x

www.rsc.org/xxxxxx

ARTICLE TYPE

Synthesis and characterization of carbon coated sponge-like tin oxide (SnO_x) films and their application as electrode materials in lithium-ion batteries

Cite this: DOI: 10.1039/x0xx00000x

Received 00th January 2015,
Accepted 00th January 2015

DOI: 10.1039/x0xx00000x

www.rsc.org/

Nils Mohri,[1§] Bernd Oschmann,[2,3§] Franziska Mueller,[4,5] Nina Laszczynski,[4,5] Jan von Zamory[4,5] Muhammad Nawaz Tahir,[1] Stefano Passerini,[4,5] Rudolf Zentel,[2,*] and Wolfgang Tremel[1,*]

Nanoporous metal oxides are widely used for the development of various functional nanostructures. We report on the synthesis of sponge-like tin oxide films on copper foil by anodization of electrochemically deposited tin films. The thin films are functionalized using a surface-anchoring carbon precursor-polymer (poly(acrylonitrile-b-dopamine acrylamide)) followed by annealing at elevated temperature to convert the polymer coating into a carbonaceous coating. The as prepared and the carbon coated films are characterized by X-ray diffraction (XRD), X-ray photoelectron spectroscopy (XPS), scanning electron microscopy (SEM) and Raman spectroscopy. Subsequently, both SnO_x films are employed as anode materials in lithium ion batteries. Carbon coating has a beneficial effect on the battery performance with respect to the rate capability, increasing the capacity by 200 mAh g^{-1} for all applied current densities. After 20 cycles, coated samples show a reversible specific charge capacity of 497 mAh g^{-1}. *Ex situ* scanning electron microscopy reveals the retention of the sponge-like morphology even after cycling.

Introduction

The interest in the synthesis of carbon-coated nanostructured materials with a high surface area has increased during the last years due to their enhanced applications in various fields such as catalysis[1,2] and electrochemical energy storage devices, especially lithium-ion batteries (LIBs).[3–6] Currently, LIBs are the leading energy storage devices for portable electronics, and attractive candidates for up-scaled applications such as electric vehicles. However, state-of-the art LIBs contain electrode materials with rather limited specific capacities, such as graphite on the anode side with a theoretical capacity of 372 mAh g^{-1}. Therefore, the exploration of new anode materials with higher specific capacities is indispensable, for instance, to increase the driving range of electric vehicles.

As alternative electrode materials, tin and tin oxides (SnO or SnO_2) have attracted interest because of their theoretical specific capacity of 993 mAh g^{-1} (Sn), 1273 mAh g^{-1} (SnO), and 1494 mAh g^{-1} (SnO_2). As conversion-alloying compounds tin oxides undergo in a first step a conversion reaction to form elemental tin and Li_2O, and in a consecutive reaction elemental tin and lithium are alloyed according to[7,8]

$$SnOx + 2xLi^+ + 2xe^- \rightarrow Sn + xLi_2O \quad (1)$$

$$Sn + yLi^+ + ye^- \leftrightarrow LiySn\ (0 \leq y \leq 4.4) \quad (2)$$

However, these oxides suffer from the irreversible formation of Li_2O and from immense volume changes during the (de-)alloying progress. Both processes lead to a capacity fading during electrochemical cycling.[9-11] Thus, for such materials their morphology was found to have a high impact on the battery performance. Current approaches to address these issues range from the use of zero-dimensional nanoparticles to three-dimensional nano-sized morphologies with hollow structures,[12-16] for instance hollow tin dioxide microspheres.[16] The motivation to create hollow structures is driven by the idea that the void space buffers the volume changes occurring during the conversion and alloying processes.[17] Nanoporous tin oxides have been investigated recently, but suffered from rather short cycling lifetime.[18–20] In addition to downsizing of active material, the application of a carbon coating of the nano-sized particles lowers the intrinsically high electrical resistance within the electrode composite, thereby improving its battery performance.[21] This has been demonstrated for numerous active materials including tin oxides.[5,9,22-24]

Herein, we report on the synthesis of a carbon-coated nanoporous SnO_x films with sponge-like morphology, which was achieved by first electrodepositing Sn directly onto a Cu foil, which served as the current collector, followed by anodization of the Sn film in aqueous medium. There is no need with this approach for adding an electrochemically inactive binding material or additional slurry preparation steps, as commonly done when making battery electrodes.[25-27] The advantage of its sponge-like morphology is the nanoporous structure, which is supposed to buffer volume changes during (de-)lithiation. In addition, the porous structure enables short diffusion pathways for the lithium ions due to its nanoscale dimensions. The nanoporous SnO_x films were functionalized with block copolymers containing an anchor block and a graphitizable block, whereby the anchor block allows the carbon precursor polymer to bind onto the SnO_x surface. Subsequent heat treatment converted the carbon precursor polymer into a carbonaceous coating.[6,24,28] Polyacrylonitrile was used as carbon source. Due to the rather low pyrolysis temperature (350 °C) a flexible carbonaceous material (best described as cyclized polyacry-

lonitrile) was obtained. A similar strategy was reported to buffer volume changes of silicon, another electrode material used as alloying anode in lithium-ion batteries.[29] In this contribution we give a detailed structural and morphological characterization of the as-synthesized as well as the carbon-coated material. Carbon-coated nanoporous SnO_x films were employed as electrodes in lithium-ion batteries. The influence of the carbon coating was investigated by comparing as-anodized and carbon-coated materials. SEM and XRD were used to investigate the structure and morphology and of the SnO_x electrodes.

Experimental

Synthesis of SnO_x sponges on copper foil. Copper foil (Schlenk) was cut into round discs with diameters of 15 mm in diameter. After each preparation step, the discs were rinsed with ultrapure water and dried in ambient atmosphere at room temperature. The passivation layer on the surface was removed by immersing the discs in a solution consisting of 52.47 wt% methanol (≥ 99.8 %, Sigma-Aldrich), 35.79 wt% 1-butanol (99 % extra pure, Acros Organics), 10.69 wt% perchloric acid (70% solution in water, Acros Organics) and 0.01 wt% ultrapure water for 30s. For electrodeposition and anodization, a setup comprising a PTFE-cylinder and a copper block as anode was used. To deposit tin on the foil, a solution consisting of 0.22 mol L^{-1} tin (II) chloride dihydrate (≥ 99.99 %, Sigma-Aldrich), tri-ammonium citrate (≥ 97 %, Alfa Aesar) and deionized water was filled into the cylinder. A constant current of 4 mA was applied for 25 min using a Voltcraft PSP 1803 voltage source. After subsequent cleaning, an aqueous solution of 5.9 wt% oxalic acid dihydrate (≥ 99.5 %, Sigma-Aldrich) was used for the anodization reaction. A constant anodic bias of 10 V was applied by a Voltcraft Digi 35 voltage source for 6 min.

Carbon coating of SnO_x Sponges. The carbon precursor block copolymer was synthesized according to a previously reported synthesis strategy.[6] Acrylonitrile (AN) was polymerized by RAFT polymerization using 2-dodecylsulfanylthiocarbonylsulfanyl-2-methyl propionic acid (DMP)[30] as chain transfer agent and α,α-azoisobutyronitrile (AIBN) as initiator. The ratio of AN:CTA:AIBN was set to be 250:1:0.1. For the block copolymerization, PAN was chosen as a macro-CTA, *N*-acryloxysuccinimide (NAS)[31] as monomer and 2,2-azobis(4-methoxy-2,4-dimethylvaleronitrile) (AMDV) as initiator. The molar ratio was NAS:PAN:AMDV = 25:1:0.2. The reaction was conducted in DMSO for 48 h at 30 °C. Finally, the reactive ester was aminolyzed by the use of dopamine hydrochloride in DMSO resulting in P(AN-b-DAAM).

^{1}H-NMR (400 MHz, DMSO-*d*6) δ [ppm] = 6.20–6.70 (d, Ar-H), 3.42 (s, CONH–CH_2), 3.14 (s, C*H* of polymer backbone), 2.03 (s, CH_2 of polymer backbone and CONH-CH-CH_2).

FT-IR: 2940 (C-H valence band), 2443 (nitrile valence band), 1702 (NH amide band), 1520 (NH deformation band), 1444, 1384, 1282, 1251 cm^{-1}.

The copper foil with the deposited SnO_x sponges was dipped into 1 mL of a 20 mg mL^{-1} solution of P(AN-b-DAAM) in DMSO. The foil was removed after 8 h from the solution and washed with DMF to remove unbound polymer. The sample was dried under vacuum and subsequently pyrolyzed. The heat treatment was conducted in two steps by first heating to 300 °C for 240 min and then heating to 350 °C for 45 min.

Structural and morphological characterization. XPS spectra were measured with a PHI 5600 Multi-Technique XPS using monochromatized Al Kα at 1486.6 eV. The crystal structure of SnO_x (coated and uncoated, non-cycled) was examined via room temperature X-ray diffraction on a Bruker D8 Discover diffractometer operated in reflection geometry with a CuK$\alpha_{1,2}$ X-ray source. Measurements of non-cycled and cycled electrodes were performed on a Bruker D8 Advance with CuKα source (λ = 0.154 nm) between 10 and 85 ° (2θ) with a step size of 0.007177°. For the investigation of the surface topography a high-vacuum mode scanning electron microscope (SEM; FEI Quanta 200 FEG Environmental-SEM) at an acceleration voltage of 15 kV was applied. For cross-section measurements, samples were embedded in PMMA using a DuroFix-2 Kit by Struers GmbH. The PMMA cylinders were cut into disks of approx. 1 mm thickness with an EXAKT 300CP diamond band saw followed by gluing the disks on plexiglas slides and polishing on a Struers Roto-Pol-31. For the polymer characterization, NMR (nuclear magnetic resonance) spectroscopy was conducted using a Bruker ARX 400, and FTIR spectroscopy (Fourier transform infrared) was carried out on a Jasco FT/IR 4100 spectrometer equipped with an ATR unit. Size exclusion chromatography (SEC) was performed with hexafluoroisopropanol as solvent. The detector system contained refractive index (Agilent) and UV-vis (Agilent) units. The calibration was done using polymethylmethacrylate standards, purchased from Polymer Standard Services.

Electrochemical characterization of SnO_x Sponge. The SnO_x electrode mass loading of was in the range of 2.77 – 3.00 mg. Swagelok^{TM}-type cells were assembled in a glove box (MBraun) with water and oxygen contents lowerthan 0.1 ppm. Polypropylene fleeces (FS2190 Freudenberg, Germany) were used as separators. They were drenched with the 1M $LiPF_6$ in ethylene carbonate: diethyl carbonate 3:7 electrolyte. Lithium foil (Rockwood Lithium) was used as counter and reference electrodes; therefore, all potentials refer to the Li/Li^+ redox couple. The electrochemical experiments were conducted at 20 °C ± 2 °C. A Maccor Battery Tester was used for galvanostatic cycling experiments. Cyclic voltammetry was performed using a VMP3 potentiostat (BioLogic), applying a sweep rate of 0.05 mV s^{-1} in a potential range of 0.01 V to 3.0 V.

Results and Discussion

Structural and morphological characterization of the carbon coated SnO_x sponges

Tin films were electrodeposited from a solution containing tin(II) chloride and tri-ammonium citrate[32] onto a copper (foil), which subsequently acted as current collector for the electrochemical tests (Fig. 1). The SEM image of the deposited tin film is shown in Fig. 2a. The surface shows a pre-structuring of tin resulting from single crystals grown together during tin deposition. The sponge-like SnO_x film (SEM image in Fig. 2b) was formed during the anodization.[33] The oxygen evolution during the anodization inhibits regular pore growth; rupturing of the pores leads to the formation of a sponge-like structure[19,33] with pore diameters of 30-60 nm and wall thicknesses of 10-15 nm (Fig. 2c).

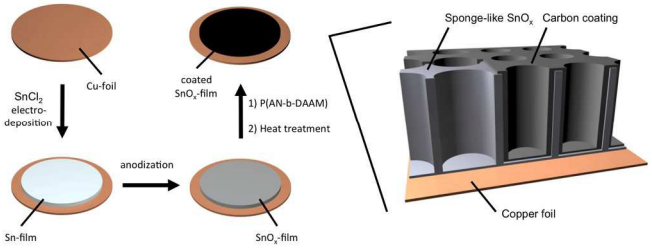

Fig. 1. Scheme showing the different steps of sample preparation (left) and magnification of the schematic sample structure (right).

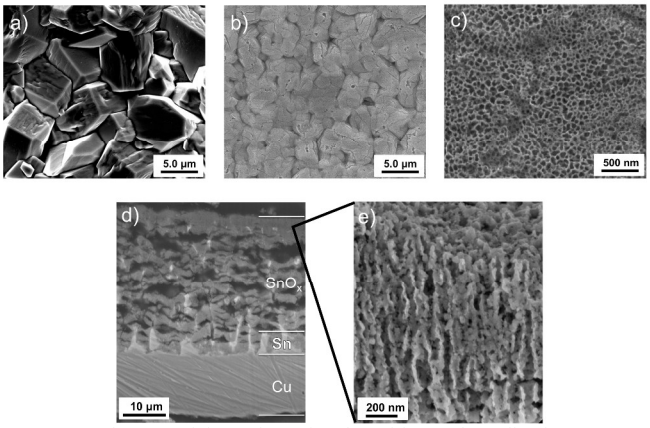

Fig. 2. SEM images of tin surface after deposition and anodization. a) Deposited metallic tin with different oriented single crystalline tin domains, b) anodized SnO_x surface, c) high resolution image of sponge-like SnOx surface. d) cross sectional image. Top: Sponge-like nanoporous SnO_x (grey), cracks from oxygen evolution breaking up into a regular tubular structure (black). Middle: Thin tin adhesion layer connecting nanoporous tin oxide to the underlying copper support. Bottom: Copper support. e) High resolution cross sectional SEM image of the SnO_x layer showing the nanoporosity.

Cross section measurement of the anodized sample showed a nanoporous SnO_x film with a thickness of 20 - 25 µm (Fig. 2d-e). Longer (> 6 min) anodization times resulted in spallation of the oxide layer, because oxygen evolution led to a detachment of the SnO_x film from the copper foil once the reaction reached the bottom of the tin layer. Thus, anodization was interrupted shortly before the copper support was reached. Thus, a thin layer of non-oxidized tin remained at the bottom of the porous tin oxide granting the adhesion to the copper foil.

The crystallinity of the film was investigated by XRD (Fig. 3). As commonly observed for SnO_x, broad reflections appeared at 26.6 ° 33.9 ° and 51.8 °, which can be attributed to SnO_2.[34-36] Sharp reflections with low intensity at 30.6 °, 32.0 °, 43.8 ° and 44.9 ° originate from the metallic Sn layer. The remaining high intensity reflections at 43.2 °, 50.3 ° and 73.9 ° can be attributed to the copper support. Reflections from SnO could not be detected due to the highly amorphous nature of the film.[37] The SnO_x layer was functionalized with a block copolymer containing a suitable anchor group. The block copolymer comprised polyacrylonitrile (PAN) as carbon precursor block and a block containing a dopamine anchor groups for metal oxide surface binding.[6,28,38] The reversible addition-fragmentation chain transfer (RAFT) polymerization based synthesis is illustrated in Fig. 4.

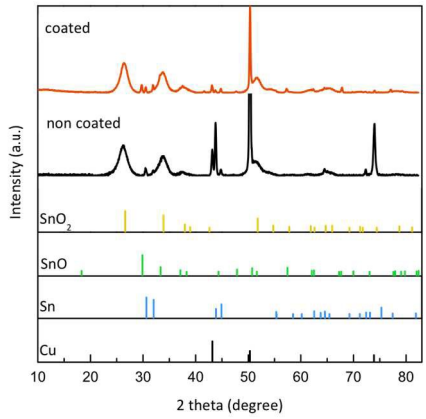

Fig. 3. XRD patterns before (black) and after coating and annealing (orange), reference patterns of SnO_2 (JCPDS 00-041-1445), SnO (JCPDS 01-085-0423), Sn (JCPDS 01-065-0296) and Cu (JCPDS 01-070-3038).

Briefly, the polyacrylonitrile block was synthesized in a first step with approx. ~70 repeat units (average) as confirmed by NMR spectroscopy (Fig. S1, Supporting Information).

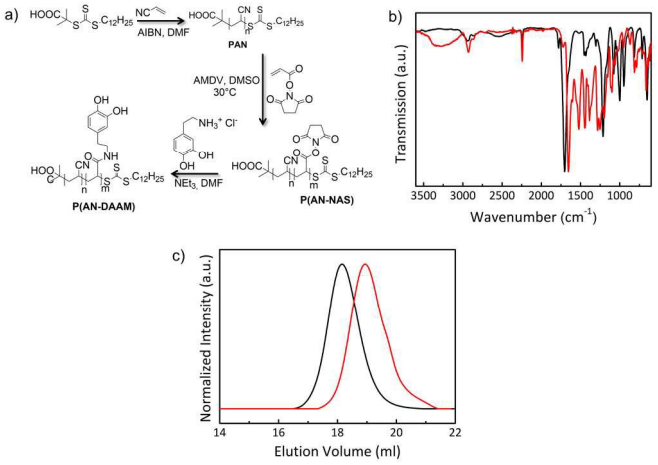

Fig. 4. a) Reaction scheme for the synthesis of P(AN-b-DAAM). b) IR spectra of P(AN-b-NAS) (black) and P(AN-b-DAAM) (red). c) SEC of P(AN) (red) and P(AN-b-DAAM) (black).

Dopamine was attached to the polymer after the block copolymerization with a reactive ester monomer (average number of reactive ester monomer repeating units ~ 23, see NMR in Fig. S2) by aminolysis of the reactive ester to obtain poly(acrylonitrile-dopamine acrylamide) (P(AN-DAAM)) in the final step. The successful synthesis of the polymer was demonstrated by FTIR spectroscopy revealing the presence of the amide band (1702 cm^{-1}) as a consequence of the attachment of dopamine unit and the disappearance of the reactive ester band (1654 cm^{-1}) (Fig. 4b). Size exclusion chromatography (SEC) showed a shift to lower elution volumes after the block copolymerization (Fig. 4c), and NMR spectroscopy further proves the attachment of dopamine (Fig. S3, Supporting Information).

After coating of the SnO_x surface with polymer and subsequent heat treatment, the structural morphology of the embedded samples appears unchanged as shown by cross-sectional SEM (Fig. S4, Supporting Information). In the X-ray diffractogram new reflections appeared at 29.8 °, 57.3 °, 62.1 °, 62.5 ° and 67.8 ° (Fig. 3), which

could be assigned to tin(II) oxide (as the heat treatment increases the crystallinity of SnO).

Energy dispersive X-ray (EDX) spectroscopy was used to further investigate the elemental composition of the sponge-like SnO_x (Fig. 5). In contrast to the constant Sn:O ratio observed for the as anodized sample, which was determined to be approx. 1:1 throughout the whole sample (Fig. 5a), the Sn:O ratio of the heat treated and carbon-coated sample was 1:1 in the vicinity of the Cu foil, but it increases when moving from the middle of the SnO_x layer towards the open surface (see Fig. 5b). The observed oxygen content gradient is in contrast with previous reports showing an increased oxidation state of SnO_x after heat treatment.[39,40] However, this is explained considering that the heat-treatment involves carbonization of the polymer coating in oxygen-free atmosphere, resulting in the generation of a reducing atmosphere.[41]

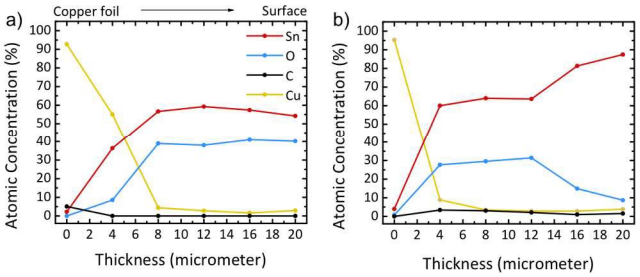

Fig. 5. EDX cross-section analysis before (a) and after coating (b). Corresponding SEM images are shown in Fig. S5 and S6.

A carbon content ranging between 2.1 % and 3.6 % is detected throughout the cross section of the coated sample (Fig. 5b), confirming the homogeneous carbon distribution within the sponge, whereas no carbon signal was detected for the uncoated sample (Fig. 5a).

The elemental composition of the film was studied by X-ray photoelectron spectroscopy (XPS). High-resolution spectra of C and Sn before and after coating and annealing are shown in Fig. 6a-b. Representative spectra are shown in Fig. 6c. For the non-coated sample, a low intensity carbon signal was detected. Since XPS is a surface sensitive technique and no carbon signal was detected in the EDX analysis we assume the signal to originate from adventitious carbon. Curve fitting reveal the typical peaks at 284.6, 286.2 and 288.9 eV resulting from C-C, C-O and C=O units, respectively.[42] After coating, an increase of 18 % in intensity was observed for the C 1s-peak, while the intensity of the Sn 3d5- and O 1s-peak decreased. A slight shift to lower binding energies indicates a lower oxidation state of the carbon as expected for the polymer. Two additional signals appear at 287.7 and 292.6 eV. The first may be attributed to C-N bonds resulting from nitrogen incorporated in the conjugated organic structure of the coating after pyrolysis.[43] A second signal originating from the C-N double bond is expected to appear at 285.9 eV. However, because of the large overlap with the C-O peak, this signal could not be resolved. Nevertheless, the increase in intensity of the C-O signal compared to the non-coated sample indicates an additional contribution from the C-N double bond in the coating. Furthermore, a N 1s peak was observed at a binding energy of 400.1 eV in the coated sample which did not appear in the uncoated one (Fig. 6d). As cyanide groups appear at lower binding energies and the peak is rather broad (FWHM = 3.4 eV), we assume it to be the result from an overlap of the C-N bond and double bond peaks as suggested by Boyd *et al.*[44] The broad, low-intensity peak at 292.6 eV is the result of π-π* transitions (shake up) in the conjugated system.

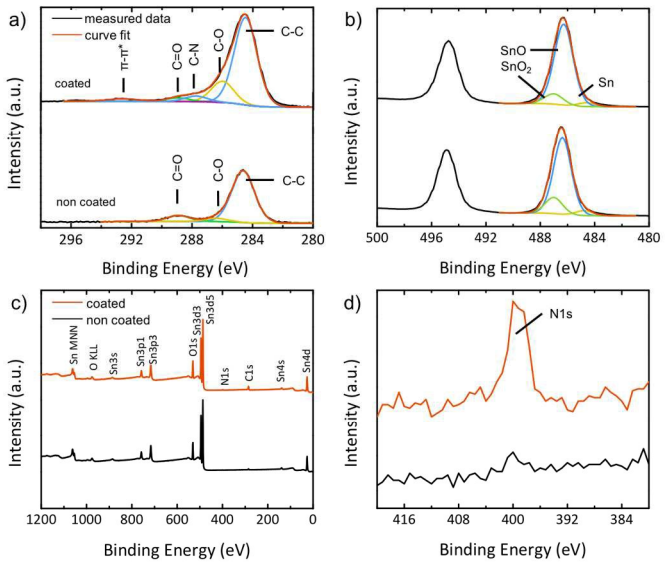

Fig. 6. XPS spectra before and after coating and annealing. (a-b) High-resolution spectra from C1s and Sn3d peaks. c) Survey spectrum of an anodized sample before (black) and after (red) coating and annealing. d) Magnification of the N1s peak from survey spectrum.

The Sn $3d^5$-signal consists of three components at 484.6, 486.3 and 487.0 eV, which could be attributed to Sn(0), Sn(II) and Sn(IV) respectively, further confirming the appearance of SnO in the sample. The ratio of $Sn/Sn^{2+}/Sn^{4+}$ was calculated to be 5%/78%/17%. The ratio of Sn to O was found to be 1:1.12, which is in good agreement with the results from EDX analysis. After carbon coating the Sn(II) signal increased to 85% while the Sn(IV) signal decreased to ≈ 11% corroborating the reduction of SnO_2 during the heat treatment.

The Raman spectrum in Fig. 7 shows the presence of two bands typically observed for carbonaceous materials, namely the D-band (1355 cm^{-1}) and the G-band (1591 cm^{-1}), which correlates to a delocalized sp^2 π -bonding.[45] As expected, none of these bands were observed for the uncoated sample.

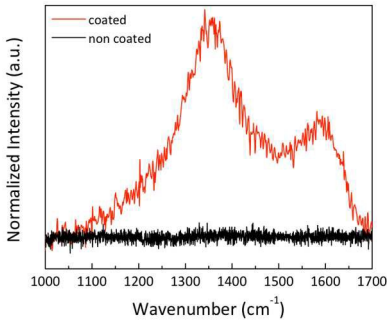

Fig. 7. Raman spectrum of the SnO_x sponge before (black) and after (red) coating. The coated sample shows the typical graphene D- and G-bands at 1355 cm^{-1} and 1591 cm^{-1}.

Electrochemical characterization of the carbon-coated SnO_x sponges.

Uncoated and coated SnO_x films were subjected to electrochemical tests (cyclic voltammetry and galvanostatic cycling). A key feature of the application of these electrodes is the fabrication process for the electrodes, as in contrast to most of the literature on tin oxide

based materials require the use of binder and carbon particle additives, [12-16] and both of these electrochemically inactive components lower the total specific capacity based on the whole electrode mass.

Fig. 8 shows the cyclic voltammetry of uncoated and coated SnO_x films. In the first cathodic sweep of the carbon-coated sponges a reduction peak at 0.9 V with a shoulder at 1.2 V was observed, which can be attributed to the partially irreversible stepwise formation of elemental Sn and Li_2O (conversion reaction) as well as the well-known solid electrolyte interphase formation due to electrolyte decomposition.[46-48] A shoulder at 0.45 V is followed by the main cathodic peak at 0.15 V, whereby the electrochemical features occurring in the range of 0.6 V to 0.01 V are attributed to the formation of Li_xSn alloys.[49,50]

The main anodic peak at 0.55 V as well as a second peak at 1.28 V, are correlated to the stepwise dealloying processes of the Li_xSn alloys.[49] The peak at 1.6 V is, however, due to the only partial reconversion of Li_2O into SnO_x and Li.[50,51] The second as well as the following cycles show some differences compared to the first cycle. The cathodic peak at 0.9 V is less pronounced, as the formation of irreversible Li_2O and SEI takes place mainly in the first cycle. Furthermore, the main cathodic signal is less pronounced. This might be explained by trapping of lithium ions within the composite resulting from structural reorganization especially occurring in the few initial cycles.[52] Upon no change was observed for the main anodic peak, the intensity of the anodic peak at 1.28 V decreased and a second peak appeared at 1.8 V also due to the decomposition of Li_2O.[9]

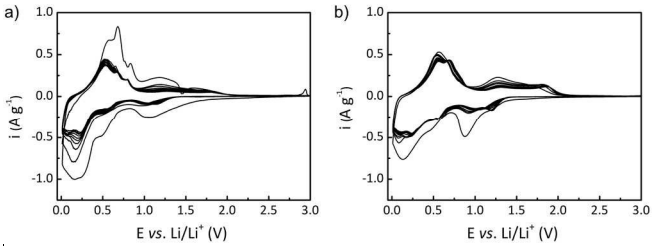

Fig. 8. Cyclic voltammograms of uncoated (a) and carbon-coated SnO_x (b).

Compared to the carbon-coated SnO_x sample, the uncoated sample shows similar features including an intense cathodic signal due to the SEI formation, a cathodic main signal due to the alloying as well as the de-alloying peaks. However, in the following cycles, the intensity of the cathodic peak at 1.2 V and the anodic peak at 1.8 V was strongly reduced. Thus, the partial decomposition of Li_2O seems to be more reversible in the presence of the carbon coating.

Fig. 9 compares the rate capability of the coated and uncoated SnO_x sponge electrodes. At the applied specific currents of 50, 100, 200 and 500 mA g^{-1} specific charge capacities of 400, 287, 220 and 102 mAh g^{-1}, respectively, were obtained for uncoated SnO_x. Significantly higher charge capacities, however, were attained by the coated SnO_x electrodes (respectively 600, 505, 431 and 260 mAh g^{-1}, i.e., more than 150 mAh g^{-1} higher), demonstrating once more the beneficial effect of the carbon coating. The coulombic efficiency in the initial cycle was low for both the uncoated (68.3 %) and the coated (60.7 %) sample due to irreversible side reactions, including the electrolyte decomposition (SEI formation) and SnO_x conversion to Sn and Li_2O. The lower efficiency of the coated sample might result from a slightly increased surface area resulting from the coating process. However, the coulombic efficiency increases rapidly for the coated material to 95.7 %, whereas the uncoated sample features coulombic efficiencies lower than 90 % for the first four cycles.

Representative potential profiles of coated and uncoated sponges for different currents densities are shown in Fig. 9b and c, which are in a good agreement with the results from cyclic voltammetry. A voltage plateau at 0.45 V was observed during the discharge and a plateau at 0.5 V during the charge due to the alloying and dealloying reactions. These plateaus are more pronounced at lower specific currents, and for the coated sample. Furthermore, in case of the coated sample a higher gain of specific capacity was observed during charge process in the region of 1.25 V to 2.0 V related to a higher reversibility of the Li_2O conversion due to the presence of the conductive carbon coating.[24] Fig. 9d shows 50 cycles of the carbon coated and uncoated SnO_x sponges at 50 mA g^{-1}. For the uncoated sponge-based electrode the charge capacity drop rapidly within the first 10 cycles from 880 to 441 mAh g^{-1}. In contrast, the initial charge capacity of the coated sample was lower (650 mAh g^{-1}), but the capacity retention was higher, as the discharge capacity after 10 cycles was still 555 mAh g^{-1}. The specific capacity for the coated sample was up to the 50th cycle, i.e., always about 120 mAh g^{-1} higher than for the uncoated material.

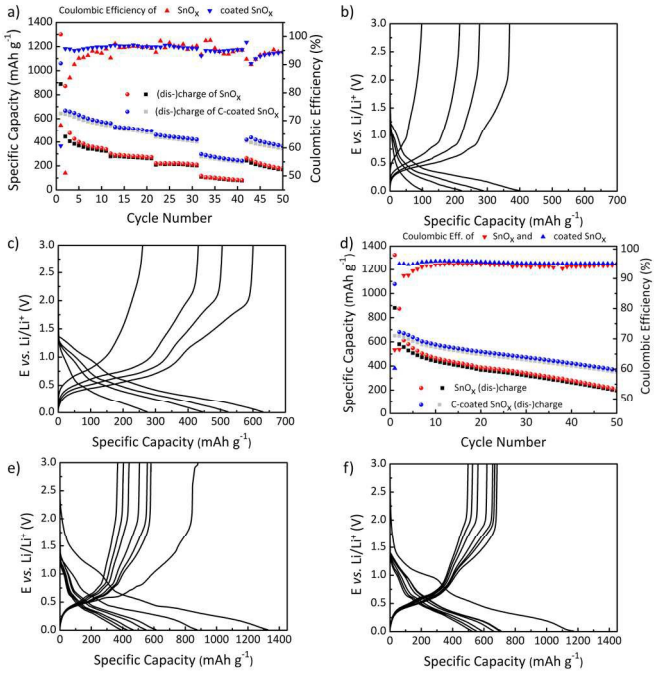

Fig. 9. C-rate performance of uncoated and carbon-coated SnO_x sponges (a) and corresponding potential profiles at the different applied specific currents of uncoated (b) and coated (c) SnO_x sponges. Shown are the cycles 5, 15, 25, and 35. (d) Cycling at a constant current density of 50 mA g^{-1}; cut-off potentials: 0.01 and 3.0 V. Potential of cycles 1, 2, 3, 5, 10, 15, 20 for uncoated SnO_x (e) and coated SnO_x (f) at 0.05 C. Cut-off potentials: 0.01 and 3.0 V *vs.* Li/Li^+.

Potential profiles of selected cycles are provided in Fig. 9 e and f. They show the enhanced cycling performance of the coated SnO_x electrodes. For the uncoated SnO_x sponge-based electrodes, the plateau of the charge profile in the voltage region between 0.5 and 0.75 V decreases. However, the decrease of the capacity above 1.0 V is more pronounced upon continuous cycling. In contrast, the plateau between 0.5 and 0.75 V related to the de-alloying reaction appears to be very reversible for the coated sample.

Electrochemical impedance spectroscopy measurements of pristine and coated samples were conducted (not shown) and only negligible differences could be observed. However, improved electrochemical performance by the application of a cyclized polyacrylonitrile coating due to enhanced mechanical properties, i.e. the ability to buffer volume changes, has been reported previously[29] and might be a possible reason for the improved performance of C-SnO_x.

Compared to previous studies on nanoporous tin oxide produced with the same methodology and reporting capacities of about 230 mAh g^{-1} after 20 cycles in the voltage range from 0.01 V to more than 2.0 V at 1C,[18] sponge-like carbon coated SnO_x showed a strongly enhanced performance as anode material for lithium-ion batteries, exhibiting a discharge capacity of 497 mAh g^{-1} after 20 cycles.

Compared with other morphologies such as hollow nanostructures, nanoboxes or nanoflowers, enhanced specific capacities could be obtained by the method reported here as demonstrated in Table S3. Additionally, it should be emphasized that the electrodes discussed in this article mainly consist of the active material (SnO_x, 95-97 wt.%) and no inactive material such as binder or carbon particles is required. In contrast to that, most previous reports apply only 70-80 wt.% active material contents (tin oxides) (see Table S3), which lowers the specific capacity of the whole electrode composite.

The morphology of the sponge-like structure was investigated after galvanostatic cycling by *ex-situ* SEM measurements (Fig. 10) for C-SnO_x samples after the first and fifth charges (delithiation). The images show the preservation of the sponge-like morphology upon continuous (dis-)charging moreover, the porous structure was still clearly observable after cycling.

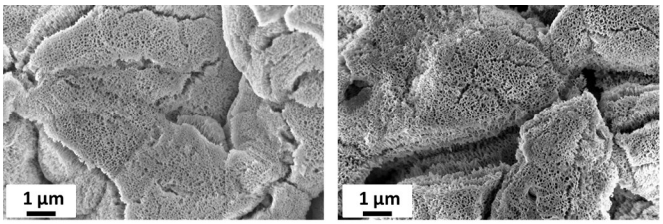

Fig. 10. SEM images of C-SnO_x electrodes after a) the 1st and b) 5th charges (delithiation) showing the preservation of the sponge-like morphology even after cycling.

Ex-situ XRD measurements were performed to confirm the electrochemical process described before for SnO_2. The XRD pattern of the first discharge (Fig. 12, see also Fig. S7) for the corresponding voltage profile) shows that SnO_x was mainly decomposed building alloying products. Due to the amorphous character of the alloy, it cannot be detected with XRD measurements, but deduced by the comparison with the electrochemical measurements (Fig. S7). Nevertheless, small fractions of Sn remain after the first discharge, indicating a certain amount of non-active material within the electrode. The XRD patterns of the first and of the fifth charge (Fig 12 and S7 for the voltage profile) show mainly Sn reflections, which is in accordance to the reversible (de-)alloying reaction.[46,59] However, no additional reflections or phases are visible after the 5th charge as the process after the 1st charge is reversible.

Conclusions

We demonstrated the synthesis of carbon-coated sponge-like SnO_x films on copper foil with enhanced performance as anode electrodes in Li-ion batteries. The porous SnO_x films were prepared by deposition and anodization of Sn layers, followed by carbon coating, using a block copolymer as carbon precursor polymer and a thermal annealing in oxygen-free environment. This procedure yields thin homogeneous carbon-coating of the SnO_x films. SEM/EDX, Raman spectroscopy and XPS confirmed the sponge-like morphology and the presence of the thin carbon film for the coated SnO_x sample while XRD and XPS showed the tin oxide film to mainly consist of tin(II) oxide prior to the coating; partial reduction was observed during the heat treatment. Electrochemical characterization of the binder- and carbon particle free elctrodes showed that the coated SnO_x sponge exhibits an increased specific capacity and higher cycling stability as compared to the non-coated sample. The porous structure of the SnO_x film could be retained even upon cycling as proven by *ex-situ* SEM measurements.

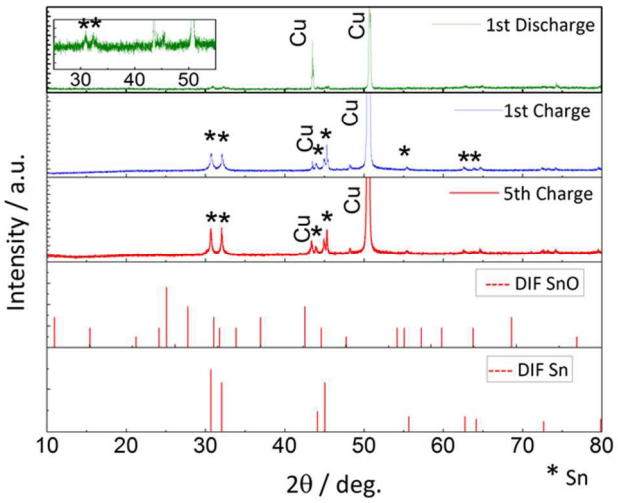

Fig. 11. XRD pattern of cycled electrodes after the first discharge, the first and the fifth charge. Reference pattern of Sn (JCPDS 00-001-0926) and SnO (JCPDS 00-013-0111).

Acknowledgements

This work was supported by the *International Research Training Group (IRTG 1404)* jointly funded by DFG and NRF, the Naturwissenschaftlich-medizinisches Forschungszentrum (NMFZ) Mainz, and the SPP 1420 funded by the Deutsche Forschungsgemeinschaft (DFG). B.O. is grateful to the graduate school MAINZ for a fellowship through the Excellence Initiative (DFG/GSC 266).

Notes and References

[1] *Institut für Anorganische Chemie und Analytische Chemie, Johannes Gutenberg Universität, Duesbergweg 10–14, 55128 Mainz, Germany, *email: tremel@uni-mainz.de*
[2] *Institut für Organische Chemie, Johannes Gutenberg Universität, Duesbergweg 10-14, 55128 Mainz, Germany, *email:zentel@uni-mainz.de*
[3] *Graduate School Materials Science in Mainz, Staudinger Weg 9, 55128, Mainz, Germany*
[4] *Helmholtz Institute Ulm (HIU), Electrochemistry I,§ Helmholtzstr. 11, 89081 Ulm, Germany*
[§] *Karlsruhe Institute of Technology (KIT), P.O. Box 3640, 76021 Karlsruhe, Germany,*
[5] *Institute of Physical Chemistry, University of Muenster, Corrensstr. 28/30, 48149 Muenster, Germany*

* *Corresponding authors*

§ Authors contributed equally to this manuscript

Electronic Supporting Information (ESI) Available: ^{1}H-NMR spectrum of polyacrylonitrile (Fig. S1), ^{1}H-NMR spectrum of poly(acrylonitrile-block-N-acryloxysuccinimide) (Fig. S2), ^{1}H-NMR spectrum of poly(acrylonitrile-block-dopamine acrylamide) showing both the typical polyacrylonitrile signals and the dopamine acrylamide signals (Fig. S3), cross-sectional SEM image of a coated SnO_x sample (Fig. S4), cross-sectional SEM image of carbon-coated SnO_x sponge (Fig. S5), cross-sectional SEM image of a carbon-coated SnO_x sponge (Fig.S6), potential profiles of cycles 1, 2, 3, 5, 10, 15, 20 for uncoated SnO_x (a) and coated SnO_x (b) at 0.05 C. Cut-off potentials: 0.01 and 3.0 V *vs.* Li/Li^+ (Fig. S7), elemental composition a coated sample (Table S1), elemental compositions of a carbon-coated sample (Table S2). See DOI:10.1039/b00000x/

1 S. Shanmugam and A. Gedanken, *Small*, 2007, **3**, 1189–1193.
2 C. Mahendiran, T. Maiyalagan, K. Scott, and A. Gedanken, *Mater. Chem. Phys.,* 2011, **128**, 341–347.
3 A. S. Aricò, P. Bruce, B. Scrosati, J.-M. Tarascon, and W. van Schalkwijk, *Nat. Mater.,* 2005, **4**, 366–377.
4 P. G. Bruce, B. Scrosati, and J.-M. Tarascon, *Angew. Chem. Int. Ed.* 2008, **47**, 2930–2946.
5 H. Li and H. Zhou, *Chem. Commun.,* 2012, **48**, 1201-1217.
6 B. Oschmann, D. Bresser, M. N. Tahir, K. Fischer, W. Tremel, S. Passerini, and R. Zentel, *Macromol. Rapid Commun.,* 2013, **34**, 1693–1700.
7 J.-M. Tarascon and M. Armand, *Nature* 2001, **414**, 359–367.
8 J. S. Chen, Y. L. Cheah, Y. T. Chen, N. Jayaprakash, S. Madhavi, Y. H. Yang, and X. W. Lou, *J. Phys. Chem., C* 2009, **113**, 20504–20508.
9 X. W. Lou, J. S. Chen, P. Chen, and L. A. Archer, *Chem. Mater.* 2009 **21**, 2868–2874.
10 D. Larcher, S. Beattie, M. Morcrette, K. Edström, J.-C. Jumas, and J.-M. Tarascon, *J. Mater. Chem.,* 2007, **17**, 3759-3772.
11 J. Besenhard, M. Hess, and P. Komenda, *Solid State Ionics,* 1990, **40-41**, 525–529.
12 L. Zhang, G. Zhang, H. B. Wu, L. Yu, and X. W. D. Lou, *Adv. Mater.,* 2013, **25**, 2589–2593.
13 X. W. Lou, L. A. Archer, and Z. Yang, *Adv. Mater.* 2008, **20**, 3987–4019.
14 J. S. Chen and X. W. D. Lou, *Small* 2013, **9**, 1877–1893.
15 C. Wang, G. Du, K. Ståhl, H. Huang, Y. Zhong, and J. Z. Jiang, *J. Phys. Chem. C* 2012, **116**, 4000–4011.
16 S. Han, B. Jang, T. Kim, S. M. Oh, and T. Hyeon, *Adv. Funct. Mater.,* 2005, **15**, 1845–1850.
17 L. Zhang, H. B. Wu, and X. Wen Lou, *Mater. Horiz.* 2013, **1**, 133-138.
18 G. F. Ortiz, P. Lavela, P. Knauth, T. Djenizian, R. Alcántara, and J. L. Tirado, *J. Electrochem. Soc.,* 2011, **158**, A1094-1099.
19 J.-W. Lee, S.-J. Park, and H.-C. Shin, *Kor. J. Mater. Res.,* 2011, **21**, 21–27.
20 S.-J. Park and H.-C. Shin, *Kor. J. Mater. Res.* 2012, **22**, 1–7.
21 M. Khan, M. N. Tahir, S. F. Adil, H. U. Khan, M. R. H. Siddiqui, A. A. Al-Warthan, and W. Tremel, *J. Mater. Chem. A* **2015**, DOI: 10.1039/C5TA02240
22 X. Ji, X. Huang, J. Liu, J. Jiang, X. Li, R. Ding, Y. Hu, F. Wu, and Q. Li, *Nanoscale Res Lett*, 2010, **5**, 649–653.
23 P. Wu, N. Du, H. Zhang, J. Yu, Y. Qi, and D. Yang, *Nanoscale,* 2011, **3**, 746–750.
24 B. Oschmann, M. N. Tahir, F. Mueller, D. Bresser, I. Lieberwirth, W. Tremel, S. Passerini, and R. Zentel, *Macromol. Rapid Commun.* 2015, **36**, 1075–1082.
25 A. Moretti, G.-T. Kim, D. Bresser, K. Renger, E. Paillard, R. Marassi, M. Winter, and S. Passerini, *J. Power Sources,* 2013, **221**, 419–426.
26 A. Magasinski, B. Zdyrko, I. Kovalenko, B. Hertzberg, R. Burtovyy, C. F. Huebner, T. F. Fuller, I. Luzinov, and G. Yushin, *ACS Appl. Mater. Interfaces,* 2010, **2**, 3004–3010.
27 J. Drofenik, M. Gaberscek, R. Dominko, F. W. Poulsen, M. Mogensen, S. Pejovnik, and J. Jamnik, *Electrochimica Acta,* 2003, **48**, 883–889.
28 D. Bresser, B. Oschmann, M. N. Tahir, F. Mueller, I. Lieberwirth, W. Tremel, R. Zentel, and S. Passerini, *J. Electrochem. Soc.* 2015, **162**, A3013-3020.
29 D. M. Piper, T. A. Yersak, S.-B. Son, S. C. Kim, C. S. Kang, K. H. Oh, C. Ban, A. C. Dillon, and S.-H. Lee, *Adv. Energy Mater.,* 2013, **3**, 697–702.
30 J. T. Lai, D. Filla, and R. Shea, *Macromolecules,* 2002, **35**, 6754–6756.
31 D. E. Bergbreiter, P. L. Osburn, and C. Li, *Org. Lett.,* 2002, **4**, 737–740.
32 A. He, Q. Liu, and D. G. Ivey, *J Mater Sci: Mater Electron*., 2008, **19**, 553–562.
33 H.-C. Shin, J. Dong, and M. Liu, *Adv. Mater.* 2004, **16**, 237–240.
34 X. Hou, Y. Hu, H. Jiang, Y. Li, W. Li, and C. Li, *J. Mater. Chem. A,* 2015, **3**, 9982–9988.
35 H. El-Shinavi, A. S. Schulze, M. Neumeier, T. Leichtweiß, J. Janek, *J. Phys. Chem.C,* 2014, **118**, 8818−8823.
36 D. M. Mukhamedshina, K. A. Mit', N. B. Beisenkhanov, E. A. Dmitriyeva, and I. V. Valitova, *J Mater Sci: Mater Electron*. 2008, **19**, 382–387.
37 L. Zaraska, N. Czopik, M. Bobruk, G. D. Sulka, J. Mech, and M. Jaskuła, *Electrochim. Acta,* 2013, **104**, 549–557.
38 M. N. Tahir, M. Eberhardt, P. Theato, S. Faiß, A. Janshoff, T. Gorelik, U. Kolb, and W. Tremel, *Angew. Chem. Int. Ed.* 2006, **45**, 908–912.
39 J.-H. Jeun, H.-S. Ryu, and S.-H. Hong, *J. Electrochem. Soc.*, 2009, **156**, J263-266.
40 A. Palacios-Padrós, M. Altomare, K. Lee, I. Díez-Pérez, F. Sanz, and P. Schmuki, *ChemElectrochem.* 2014, **1**, 1133–1137.
41 K. Xie, Z. Lu, H. Huang, W. Lu, Y. Lai, J. Li, L. Zhou, and Y. Liu, *J. Mater. Chem.,* 2012, **22**, 5560-5567.
42 T. L. Barr, *J. Vac. Sci. Technol. A,* 1995, **13**, 1239-1246.
43 J. F. Moulder and J. Chastain, *Handbook of x-ray photoelectron spectroscopy. A reference book of standard spectra for identification and interpretation of XPS data*, Physical Electronics Division, Perkin-Elmer Corp., Eden Prairie, Minn, ©1992.
44 K. J. Boyd, *J. Vac. Sci. Technol. A,* 1995, **13**, 2110-2122.
45 A. C. Ferrari and J. Robertson, *Phil. Trans. Royal Soc. A: Math. Phys. Eng. Sci.,* 2004, **362**, 2477–2512.
46 I. A. Courtney and J. R. Dahn, *J. Electrochem. Soc.,* 1997, **144**, 2045-2052.
47 Z. Wen, F. Zheng, H. Yu, Z. Jiang, and K. Liu, *Mater. Charact.,* 2013, **76**, 1–5.
48 E. Peled, *J. Electrochem. Soc.,* 1979, **126**, 2047-2051.
49 X. W. Lou, C. M. Li, and L. A. Archer, *Adv. Mater.,* 2009, **21**, 2536–2539.
50 M. Mohamedi, S.-J. Lee, D. Takahashi, M. Nishizawa, T. Itoh, and I. Uchida, *Electrochim. Acta,* 2001, **46**, 1161–1168.
51 T. Brousse, R. Retoux, U. Herterich, and D. M. Schleich, *J. Electrochem. Soc.,* 1998, **145**, 1-4.
52 D. Bresser, F. Mueller, D. Buchholz, E. Paillard, and S. Passerini, *Electrochimica Acta,* 2014, **128**, 163–171.
53 J. W. Lee, S.-J. Park, and H.-C. Shin, *Kor. J. Mater. Res*. 2011, **21**, 21-27.
54 X. W. Lou, Y. Wang, C. Yuan, J. Y. Lee, and L. A. Archer, *Adv. Mater.* 2006, **18**, 2325-2329.
55 Z. Wang, D. Luan, F. Y. C. Boey, and X. W. Lou, *J. Am. Chem. Soc*. 2011, **133**, 4738-4741.
56 M.-S. Park, G.-X. Wang, Y.-M. Kang, D. Wexler, S.-X. Dou, and H.-K. Liu, *Angew. Chem. Int. Ed*. 2007, **46**, 750–753.
57 L. Yuan, J. Wang, S. Y. Chew, J. Chen, Z. P. Guo, L. Zhao, K. Konstantinov, JH. K. Liu, *J. Power Sources* 2007, **174**, 1183-1187.
58 J. Ning, Q. Dai, T. Jiang, K. Men, D. Liu, N. Xiao, C. Li, D. Li, B. Liu, B. Zou, G. Zou, and W. W. Yu, *Langmuir* 2009, **25**, 1818-1821
59 K. Furuya, K. Ogawa, Y. Mineo, A. Matsufuji, J. Okuda, and T. Erata, *J. Phys.: Condens. Matter,* 2001, **13**, 3519–3532.

Graphical abstract